JOURNAL OF SOLID STATE CHEMISTRY 116, 77–86 (1995)

Two New Barium–Vanadium(IV) Phases: $Ba(VO)_2(SeO_3)_2(HSeO_3)_2$, the First Barium Vanadium Selenite, and $Ba_8(VO)_6(PO_4)_2(HPO_4)_{11} \cdot 3H_2O$, a Compound Built Up from Two Types of One-Dimensional Chains

William T. A. Harrison,* J. T. Vaughey,*,[1] Allan J. Jacobson,*,[2] David P. Goshorn,† and Jack W. Johnson†

*Department of Chemistry, University of Houston, Houston, Texas 77204-5641; and †Corporate Research Laboratories, Exxon Research and Engineering Company, Annandale, New Jersey 08801

Received May 16, 1994; in revised form September 6, 1994; accepted September 7, 1994

The hydrothermal syntheses, X-ray single-crystal structures, and some properties of $Ba(VO)_2(SeO_3)_2(HSeO_3)_2$ and $Ba_8(VO)_6(PO_4)_2(HPO_4)_{11} \cdot 3H_2O$ are described. $Ba(VO)_2(SeO_3)_2(HSeO_3)_2$ contains a three-dimensional network of VO_6 and $(H)SeO_3$ polyhedra, linked via V–O–Se bonds. The Ba cation is 10-coordinate, the VO_6 group contains a short vanadyl V=O bond typical of V^{IV}, and the $(H)SeO_3$ groups are pyramidal. Magnetic susceptibility data are consistent with V^{IV} and show paramagnetic behavior from 4 to 300 K. Crystal data for $Ba(VO)_2(SeO_3)_2(HSeO_3)_2$: $M_r = 781.06$, monoclinic, space group $P2_1/c$ (No. 14), $a = 9.680(3)$ Å, $b = 7.024(2)$ Å, $c = 9.882(4)$ Å, $\beta = 116.42(3)°$, $V = 601.75$ Å^3, $Z = 2$, $R = 3.89\%$, $R_w = 3.64\%$ [1637 observed reflections with $I > 3\sigma(I)$]. $Ba_8(VO)_6(PO_4)_2(HPO_4)_{11} \cdot 3H_2O$ contains a complex network of VO_6 and PO_4/HPO_4 groups, which form two different types of one-dimensional chains: one chain contains fairly regular $V^{IV}O_6$ and $(H)PO_4$ groups; the other is built up from distorted $V^{IV}O_6$ octahedra and (hydrogen) phosphate groups. 10- and 13-coordinate Ba^{2+} cations complete the structure, which shows antiferromagnetic ordering of the V^{IV} centers at ~20 K. Crystal data for $Ba_8(VO)_6(PO_4)_2(HPO_4)_{11} \cdot 3H_2O$: $M_r = 2800.05$, monoclinic, space group $C2/m$ (No. 12), $a = 31.685(11)$ Å, $b = 5.208(2)$ Å, $c = 7.784(3)$ Å, $\beta = 90.59(3)°$, $V = 1284.5(7)$ Å^3, $Z = 1$, $R = 4.03\%$, and $R_w = 5.28\%$ [1892 observed reflections with $I > 3\sigma(I)$].

INTRODUCTION

Materials containing microporous frameworks built up from units other than just tetrahedra are currently of interest (1–3), especially with respect to their potentially useful physical properties which might complement those of aluminosilicate zeolite molecular sieves. A notable family of molybdenophosphate (MoPO) phases has been characterized by Haushalter and co-workers (4): Some of these MoPOs are analogues of known structures, but many form new framework types (5). The possibility of different oxidation states for the Mo cation is an important feature of MoPO structural chemistry (5). In these MoPO materials, the Mo cation usually adopts octahedral coordination.

A system with structural possibilities similar to MoPO's is the vanadium–phosphate (VPO) combination. Vanadium may exist in oxidation states III, IV, and V in the solid state, and may adopt square pyramidal, octahedral, or even tetrahedral coordination, leading to a great variety of potential polyhedral connectivities. New VPO phases may complement known vanadium phosphates, including layered materials such as $VOPO_4 \cdot 2H_2O$ (6), which undergoes a novel redox/intercalation reaction (7), leading to new structures such as $Na_{1/2}VOPO_4 \cdot 2H_2O$ (8). When metallic (9) or organic cations (10) are combined with vanadium and phosphate, a vast variety of *M*/V/P/O materials are possible (11–13).

In this paper we report the preparations, crystal structures, and some properties of two new barium/vanadium phases. $Ba(VO)_2(SeO_3)_2(HSeO_3)_2$ is the first cation–vanadium(IV)–selenite phase to be characterized, and indicates the structural possibilities of a vertex-linked, anionic, octahedral/*pyramidal* network. $VOSeO_3 \cdot H_2O$ [vanadium(IV)] was previously characterized (14) and has a crystal structure related to the layered vanadium hydrogen phosphate, $VOHPO_4 \cdot \frac{1}{2}H_2O$ (15). $Ba_8(VO)_6(PO_4)_2(HPO_4)_{11} \cdot 3H_2O$ has a complex structure containing two distinct types of chains of vertex-linked $V^{IV}O_6$ octahedral and $(H)PO_4$ tetrahedral groups.

SYNTHESIS AND PHYSICAL CHARACTERIZATION

Green, platy, single crystals of $Ba(VO)_2(SeO_3)_2(HSeO_3)_2$ were prepared in approximately 75% yield from

[1] Present address: Department of Chemistry, Iowa State University, Ames, IA 50011.

[2] To whom correspondence should be addressed.

0022-4596/95 $6.00

a reaction mixture of initial composition 0.4 g V_2O_5 (98 + %, Aldrich), 0.045 g V (99.5%, Aldrich), 0.693 g $Ba(OH)_2 \cdot 8H_2O$ (99.9%, Aldrich), 2.0 g SeO_2 (99%, Aldrich), and 10 ml of distilled water. The reactants were sealed in a Teflon-lined Parr hydrothermal bomb and heated to 200°C for 4 days. The bomb was then slowly cooled to room temperature over a 2-day period, and the contents of the bomb recovered by vacuum filtration. $Ba(VO)_2(SeO_3)_2(HSeO_3)_2$ is air-stable.

Single crystals of $Ba_8(VO)_6(PO_4)_2(HPO_4)_{11} \cdot 3H_2O$ were synthesized from the reaction of 0.220 g V_2O_5 (98 + %, Aldrich), 0.0137 g V (99.5%, Aldrich), 0.6 ml H_3PO_4 (85%, Fisher), 0.846 g $Ba(OH)_2 \cdot 8H_2O$ (99.9%, Aldrich), and 10 ml of distilled water. This mixture was heated to 230°C for 4 days in a 23-ml Parr bomb, and then cooled to ambient temperature over a 2-day period. Vacuum filtration recovered a ~75% yield of intergrown green plates, which appear to be indefinitely stable in air.

Preliminary X-ray powder data for both phases revealed complex, low-symmetry patterns unlike those of other (Ba)/V/(P/Se)/O phases or of the reaction starting materials. "Autoindexing" attempts were inconclusive. Thermogravimetric analysis (TGA) for $Ba(VO)_2(SeO_3)_2(HSeO_3)_2$ was carried out on a small sample isolated from the reaction noted above. The sample was heated to 600°C under flowing oxygen, with a ramp rate of 2°C/min. The observed weight loss of 56.9(2)% (calc. 57.1%) corresponded to the complete transformation of $Ba(VO)_2(SeO_3)_2(HSeO_3)_2$ to a physical mixture of $Ba_3V_2O_8$ and V_2O_5, as confirmed by powder X-ray analysis of the post-TGA residue. TGA data for $Ba_8(VO)_6(PO_4)_2(HPO_4)_{11} \cdot 3H_2O$ were collected on a DuPont 9900 system: An overall 4.8(2)% weight loss resulted, in two steps, between 470 and 500°C, in fair agreement with the weight loss calculated (5.2%) for the transition:

$$Ba_8(VO)_6(PO_4)_2(HPO_4)_{11} \cdot 3H_2O \xrightarrow{\Delta} \text{“}Ba_8V_6P_{13}O_{52.5}\text{”} + 8\tfrac{1}{2}H_2O.$$

Infrared data for $Ba(VO)_2(SeO_3)_2(HSeO_3)_2$ and $Ba_8(VO)_6(PO_4)_2(HPO_4)_{11} \cdot 3H_2O$ were collected on a Galaxy FTIR 5000 Series spectrometer, using a standard KBr pellet method in each case. Magnetic susceptibility data for $Ba(VO)_2(SeO_3)_2(HSeO_3)_2$ (51.3 mg of isolated single crystals) and $Ba_8(VO)_6(PO_4)_2(HPO_4)_{11} \cdot 3H_2O$ (16.7 mg of crystals) were obtained between 4.2 and 300 K in an applied field of 6 kG using a Quantum Design Model MPMS SQUID magnetometer. Ferromagnetic impurity contributions to the magnetic susceptibility were measured and corrected for by using magnetization isotherms obtained at 77 and 298 K.

CRYSTAL STRUCTURE DETERMINATION

The crystal structure of $Ba(VO)_2(SeO_3)_2(HSeO_3)_2$ was determined from single-crystal X-ray diffraction data: A light-green, irregular plate (dimensions ~0.4 × 0.3 × 0.02 mm) was mounted on a thin glass fiber with cyanoacrylate adhesive, and room-temperature [25(2)°C] intensity data were collected on an Enraf-Nonius CAD4 automated 4-circle diffractometer (graphite-monochromated Mo$K\alpha$ radiation, λ = 0.71073 Å). After locating and centering 25 reflections ($8° < 2\theta < 17°$), the unit cell constants were optimized by a least-squares refinement, resulting in monoclinic lattice parameters of a = 9.680(3) Å, b = 7.024(2) Å, c = 9.882(4) Å, and β = 116.42(3)° (esd's in parentheses). Intensity data were collected in the ω-2θ scanning mode with standard reflections monitored for intensity changes throughout the course of the experiment (negligible variation observed). The scan speed varied from 1.1°–3.4°/min with a scan range of 0.9 + 0.35 tan θ, extended by 25% on either side of the peak for background determination, for a total of 2546 data collected ($2\theta < 70°$; $-15 \le h \le 13$, $0 \le k \le 11$, $0 \le l \le 12$). The systematic absences in the reduced data ($h0l$, $l \neq 2n$; $0k0$, $k \neq 2n$) indicated space group $P2_1/c$ (No. 14).

The crystal-structure model of $Ba(VO)_2(SeO_3)_2(HSeO_3)_2$ was developed in space group $P2_1/c$, with heavy-atom positions (Ba, V, Se) located using the direct-methods program SHELXS-86 (16). The oxygen-atom positions were located from Fourier difference maps during the refinement. After isotropic refinement, an empirical absorption correction (DIFABS) (17) was applied (minimum correction = 0.90, max = 1.51). The final cycles of full-matrix least-squares refinement were against F and included anisotropic temperature factors (isotropic for H) and a Larson-type secondary extinction correction (18) [refined value: 10(2)]. The H-atom position was located geometrically [d(O–H) = 0.95 Å], and complex, neutral-atom scattering factors were obtained from the "International Tables" (19). At the end of the refinement, residuals of R = 3.89% and R_w = 3.64% ($w_i = 1/\sigma_i^2$) resulted, and analysis of the various trends in F_o versus F_c revealed no unusual effects. The least-squares, Fourier, and subsidiary calculations were performed using the Oxford CRYSTALS system (20), running on a DEC MicroVAX 3100 computer. Crystallographic data for $Ba(VO)_2(SeO_3)_2(HSeO_3)_2$ are summarized in Table 1.

The crystal structure of $Ba_8(VO)_6(PO_4)_2(HPO_4)_{11} \cdot 3H_2O$ was established in similar fashion: A platy crystal, of dimensions ~0.4 × 0.3 × 0.03 mm, was mounted on a thin glass rod with epoxy cement, and room temperature [25(2)°C] intensity data were collected on a Siemens/Nicolet automated 4-circle diffractometer (graphite-monochromated Mo$K\alpha$ radiation, λ = 0.71073 Å). After locating and centering 26 reflections ($15° < 2\theta < 29°$), unit cell

TABLE 1
Crystallographic Parameters

	$Ba(VO)_2(SeO_3)_2(HSeO_3)_2$	$Ba_8(VO)_6(PO_4)_2(HPO_4)_{11}\cdot 3H_2O$
Empirical formula	$Ba_1Se_4V_2O_{14}H_2$	$Ba_8V_6P_{13}O_{61}H_{17}$
Formula wt.	781.06	2800.05
Habit	Light green plate	Green plate
Crystal system	Monoclinic	Monoclinic
a(Å)	9.680(3)	31.685(11)
b (Å)	7.024(2)	5.208(2)
c (Å)	9.882(4)	7.784(3)
β(°)	116.42(3)	90.59(3)
V (Å^3)	601.75	1284.5
Z	2	1
Space group	$P2_1/c$ (No. 14)	$C2/m$ (No. 12)
T (°C)	25(2)	25(2)
λ(Mo$K\alpha$) (Å)	0.71073	0.71073
ρ_{calc} (g/cm^3)	4.31	3.62
μ (Mo$K\alpha$) (cm^{-1})	167.70	75.72
Absorption corr.	DIFABS	ψ-scan
Extinction corr.	10(2)	21(2)
Min., Max. $\Delta\rho$ (e/Å)	−1.43, +2.21	−1.75, +3.27
Total data	2546	2071
Observed data[a]	1637	1892
Parameters	98	127
$R(F)$[b] (%)	3.89	4.03
$R_w(F)$[c] (%)	3.64	5.28

[a] $I > 3\sigma(I)$.
[b] $R = 100 \times \Sigma||F_o| - |F_c||/\Sigma|F_o|$.
[c] $R_w = 100 \times [\Sigma w(|F_o| - |F_c|)^2/\Sigma w|F_o|^2]^{1/2}$, with $w_i = 1/\sigma_i^2$.

constants were optimized by least-squares refinement, resulting in monoclinic lattice parameters of a = 31.685(11) Å, b = 5.208(2) Å, c = 7.784(3) Å, and β = 90.59(3)° (esd's in parentheses). Intensity data were collected in the ω-2θ scanning mode with standard reflections monitored for intensity changes throughout the course of the experiment (< ±2% variation observed). The scan speed varied from 1.5°–14.7°/min, and a total of 2071 intensity maxima were scanned ($2\theta < 60°$; $-44 \le h \le 44$, $0 \le k \le 7$, $0 \le l \le 10$). The systematic absences in the reduced data (hkl, $h + k \neq 2n$; $h0l$, $h \neq 2n$; $0kl$, $k \neq 2n$) indicated space groups $C2$ (No. 5) or $C2/m$ (No. 12).

The structure of $Ba_8(VO)_6(PO_4)_2(HPO_4)_{11}\cdot 3H_2O$ was successfully developed in the centrosymmetric space group $C2/m$, which was assumed for the remainder of the crystallographic analysis. Initial heavy-atom positions (Ba, V) were located by using SHELXS-86, and the P and O atom positions were located from Fourier difference maps during the refinement. The final cycles of full-matrix least-squares refinement were against F and included anisotropic temperature factors (isotropic for the disordered species) and a Larson-type secondary extinction correction [refined value: 21(2)]. Complex, neutral-atom scattering factors were obtained from the "International Tables." Some of the atom positions were disordered, as noted below, and no hydrogen-atom positions could be definitively located. Reducing the crystal symmetry to $C2$ was tried, but this led to unstable refinements, and did not resolve the disorder problems. At the end of the refinement (software: CRYSTALS), residuals of R = 4.03% and R_w = 5.28% ($w_i = 1/\sigma_i^2$) resulted; analysis of the various trends in F_o versus F_c revealed no unusual effects. Crystallographic data for $Ba_8(VO)_6(PO_4)_2(HPO_4)_{11}\cdot 3H_2O$ are summarized in Table 1.

Crystal Structure of $Ba(VO)_2(SeO_3)_2(HSeO_3)_2$

Final atomic positional and equivalent isotropic thermal parameters for $Ba(VO)_2(SeO_3)_2(HSeO_3)_2$ are listed in Table 2, with selected bond distance/angle data given in Table 3. $Ba(VO)_2(SeO_3)_2(HSeO_3)_2$ is a three-dimensional phase built up from vertex-sharing VO_6 and $(H)SeO_3$ units. The V/Se/O asymmetric unit and labeling scheme of $Ba(VO)_2(SeO_3)_2(HSeO_3)_2$ is shown in Fig. 1, and the complete crystal structure is illustrated in Fig. 2.

$Ba(VO)_2(SeO_3)_2(HSeO_3)_2$ is the first example of a barium–vanadium(IV)–selenite, and the component species (1 Ba, 1 V, 2 Se, 7 O, 1 H) show typical crystallochemical behavior. The barium cation (site symmetry $\bar{1}$) is coordinated by 10 oxygen atoms within 3 Å, with a d_{av}(Ba–O) of 2.877(2) Å, in tetra-capped octahedral geometry (Fig. 3): the four capping oxygen atoms [O(2), O(2′), O(5), O(5′)] form the in-layer Ba–O bonds described below, while the three bonds to O(3), O(4), and O(6) [and O(3′), O(4′), and O(6′)] bond to the V/Se/O layer above (below).

The vanadium cation [d_{av}(V–O) = 1.989(3) Å] shows a short vanadyl V=O bond (d = 1.614(6) Å), characteristic of V^{IV} or V^{V} (11), and its other five oxygen-atom vertices are connected to nearby Se cations (θ_{av}(V–O–Se) = 126°). Vanadium(IV) was assigned to the oxidation state of this atom based on several experimental criteria: The green color of $Ba(VO)_2(SeO_3)_2(HSeO_3)_2$ is typical of V^{IV}-con-

TABLE 2
Atomic Positional and Thermal Parameters for $Ba(VO)_2(SeO_3)_2(HSeO_3)_2$

Atom	x	y	z	U_{eq}[a]
Ba(1)	½	0	½	0.0100
V(1)	0.7053(1)	0.0293(2)	−0.0552(1)	0.0073
Se(1)	1.05587(9)	−0.0739(1)	0.18986(8)	0.0089
Se(2)	0.68640(8)	0.0080(1)	0.25328(7)	0.0070
O(1)	0.9281(6)	0.0912(7)	0.0826(5)	0.0091
O(2)	0.6509(6)	0.1529(7)	0.1023(6)	0.0088
O(3)	0.4946(6)	0.0666(8)	−0.2182(5)	0.0118
O(4)	0.7212(6)	0.3384(7)	−0.1033(5)	0.0100
O(5)	0.7740(6)	−0.0218(7)	−0.2182(5)	0.0084
O(6)	0.6962(6)	−0.1880(7)	−0.0066(6)	0.0125
O(7)	1.0529(6)	−0.0016(7)	0.3568(6)	0.0135
H(1)	1.1327(6)	−0.0580(7)	0.4439(6)	0.0200[b]

[a] U_{eq} (Å^2) = $(U_1U_2U_3)^{1/3}$.
[b] U_{iso} (Å^2) (not refined).

TABLE 3
Bond Distances (Å) and Angles (°) for $Ba(VO)_2(SeO_3)_2(HSeO_3)_2$

Ba(1)–O(2) × 2	2.791(5)	Ba(1)–O(3) × 2	2.847(5)
Ba(1)–O(4) × 2	2.977(5)	Ba(1)–O(5) × 2	2.871(5)
Ba(1)–O(6) × 2	2.920(5)		
V(1)–O(1)	2.020(5)	V(1)–O(2)	2.045(5)
V(1)–O(3)	1.975(5)	V(1)–O(4)	2.243(5)
V(1)–O(5)	2.030(5)	V(1)–O(6)	1.614(5)
Se(1)–O(1)	1.683(5)	Se(1)–O(5)	1.683(5)
Se(1)–O(7)	1.738(5)	Se(2)–O(2)	1.710(5)
Se(2)–O(3)	1.710(5)	Se(2)–O(4)	1.691(5)
O(4)–H(1)	1.74[a]	O(7)–H(1)	0.95
O(1)–V(1)–O(2)	87.4(2)	O(1)–V(1)–O(3)	157.9(2)
O(2)–V(1)–O(3)	92.4(2)	O(1)–V(1)–O(4)	77.4(2)
O(2)–V(1)–O(4)	79.4(2)	O(3)–V(1)–O(4)	80.9(2)
O(1)–V(1)–O(5)	86.8(2)	O(2)–V(1)–O(5)	164.9(2)
O(3)–V(1)–O(5)	87.7(2)	O(4)–V(1)–O(5)	85.7(2)
O(1)–V(1)–O(6)	100.7(2)	O(2)–V(1)–O(6)	96.2(2)
O(3)–V(1)–O(6)	101.2(3)	O(4)–V(1)–O(6)	175.2(2)
O(5)–V(1)–O(6)	98.6(2)		
O(1)–Se(1)–O(5)	102.7(2)	O(1)–Se(1)–O(7)	94.5(2)
O(5)–Se(1)–O(7)	98.8(2)	O(2)–Se(2)–O(3)	102.5(2)
O(2)–Se(2)–O(4)	103.9(2)	O(3)–Se(2)–O(4)	99.8(3)
V(1)–O(1)–Se(1)	122.8(3)	V(1)–O(2)–Se(2)	113.1(2)
V(1)–O(3)–Se(2)	135.9(3)	V(1)–O(4)–Se(2)	142.0(3)
V(1)–O(5)–Se(1)	116.1(3)		

[a] H-bond contact.

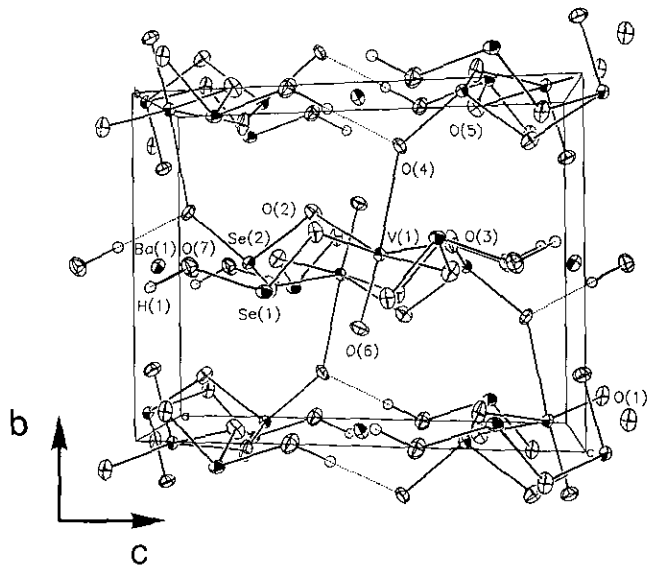

FIG. 2. Unit-cell packing of $Ba(VO)_2(SeO_3)_2(HSeO_3)_2$, viewed approximately down [100], showing the pseudo-[010] sheet structure, connected via O(4) centers (dotted lines indicate H bonds; Ba–O bonds not shown).

taining phases (21), and the magnetic susceptibility data (*vide infra*) are completely in accordance with isolated d^1 sites. A Brese–O'Keefe bond valence sum (BVS) calculation (22) found a BVS of 4.2 for the vanadium atom, and consideration of charge-balancing criteria also indicated vanadium(IV), with no evidence for partial occupancy of the other atomic sites, or any other features which would indicate the presence of vanadium(V) at the V-atom site.

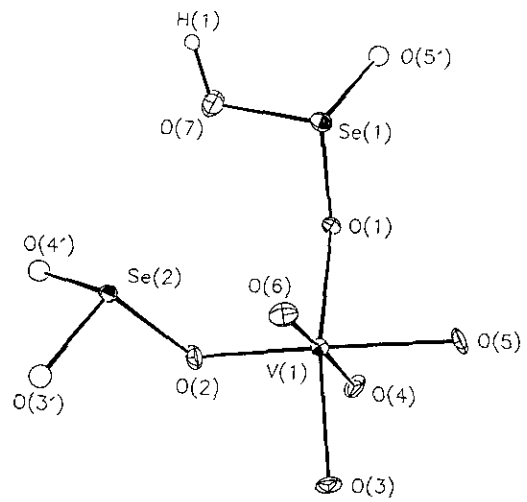

FIG. 1. ORTEP view of the V/Se/O asymmetric unit of $Ba(VO)_2(SeO_3)_2(HSeO_3)_2$, showing the atom-labeling scheme (50% thermal ellipses; arbitary radius for proton).

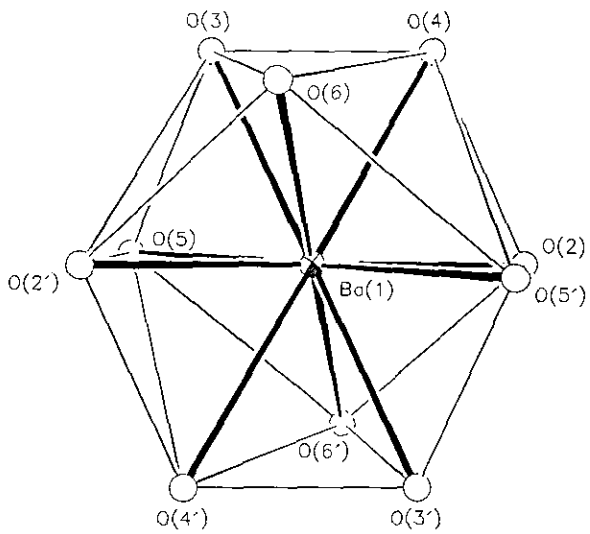

FIG. 3. Ba(1) coordination polyhedron in $Ba(VO)_2(SeO_3)_2(HSeO_3)_2$, with nonbonding O···O contacts <4.0 Å indicated by thin lines (see text). O atoms are represented by spheres of arbitrary radius.

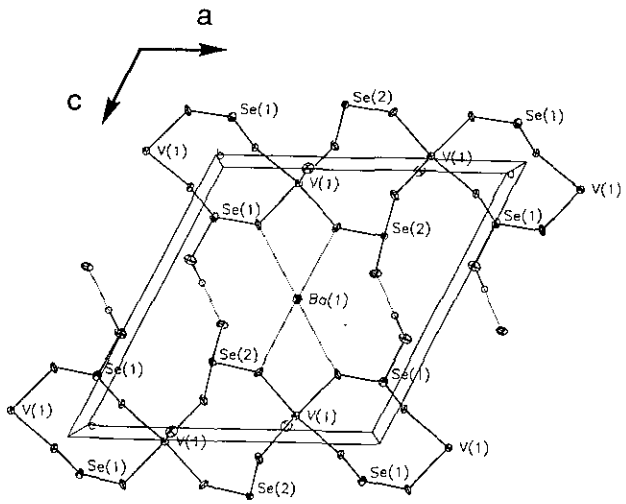

FIG. 4. [101] slice of the crystal structure of $Ba(VO)_2(SeO_3)_2(HSeO_3)_2$, at $y \sim 0$, showing the V/Se/O chains propagating in the **a**-direction, crosslinked by H bonds and links to the Ba cation (dotted lines).

Thus, $Ba(VO)_2(SeO_3)_2(HSeO_3)_2$ contains vanadium only in the V^{IV} oxidation state.

Both selenium atoms are three-coordinate by oxygen atoms, and show the characteristic SeO_3 pyramidal configuration, with the missing tetrahedral vertex occupied by the Se^{IV} lone pair. Se(1) makes two Se–O–V links, and one terminal Se–OH bond, and Se(2) makes three Se–O–V bonds. The average Se–O distance of 1.703(3) Å is typical, and the Se–OH bond is somewhat lengthened, as observed in other hydrogen selenite groups (23–25). A structurally significant H bond is formed by the Se–OH entity (see below).

The polyhedral connectivity in $Ba(VO)_2(SeO_3)_2(HSeO_3)_2$ leads to a three-dimensional V/Se/O network incorporating the "guest" Ba^{2+} cations. The structure (Fig. 4) includes pseudo-one-dimensional strings of adjacent VO_6 groups linked by pairs of Se(1) or Se(2) selenite groups, which propagate in the **a**-direction. These strings are crosslinked via Se(1)–O(7)–H(1)· · ·O(4)–Se(2) H-bonding, and Ba–O bonds, forming sheets in the [101] plane. Finally, these sheets are connected to each other in the **b**-direction by V(1)–O(4)–Se(2) bonds, and additional Ba–O links, completing the three-dimensional structure. The layers are offset with respect to each other in the [101] plane, and there are no particular channels apparent in the V/Se/O network in $Ba(VO)_2(SeO_3)_2(HSeO_3)_2$. This structure is more closely related to layered V/P/O materials than to three-dimensional microporous "zeolitic" frameworks.

Crystal Structure of $Ba_8(VO)_6(PO_4)_2(HPO_4)_{11} \cdot 3H_2O$

Final atomic positional/thermal parameters for $Ba_8(VO)_6(PO_4)_2(HPO_4)_{11} \cdot 3H_2O$ are presented in Table 4, with selected geometrical data given in Tables 5 and 6. The asymmetric units and complete structures of $Ba_8(VO)_6(PO_4)_2(HPO_4)_{11} \cdot 3H_2O$ are illustrated in Figs. 5 and 6 respectively. $Ba_8(VO)_6(PO_4)_2(HPO_4)_{11} \cdot 3H_2O$ is a complex phase built up from $V^{IV}O_6$ and $(H)PO_4$ groups. There are 2 crystallographically distinct Ba cations (10- and 13-coordinated), 2 octahedral vanadium centers, 4 phosphorus atoms, and 13 oxygen atoms. Some of these atomic species are disordered, as shown in Table 4.

Ba(1) is 10-coordinated by oxygen-atom neighbors, with a d_{av} (Ba–O) of 2.872(2) Å, and a BVS of 2.20. Its coordination approximates a pentagonal antiprism (Fig. 7), although the Ba(1) site symmetry is only *m* (through atoms O(3), Ba(1), and O(9″) at $y = \frac{1}{2}$). Ba(2) is 13-coordinated by nearby oxygen atoms within 3.1 Å, in roughly "5 + 5 + 3" geometry, with an average Ba–O contact of 2.919(5) Å. The Brese–O'Keefe BVS value for this atom is significantly greater than 2.00 (2.64), mostly because of the very short Ba(2)–O(21) bond length. Atom O(21) is part of the disordered $P(4)O_4$ group, and its location is less certain than the other atoms bound to Ba(2); thus this BVS value should be treated with caution. The Ba(2) site symmetry is also *m*; atoms Ba(2), O(10), O(11), and O(21) sit on the mirror plane at $y = 0$ (Fig. 8). Adjacent Ba(1) atoms are linked via O(9) into infinite double chains

TABLE 4
Atomic Positional and Thermal Parameters for $Ba_8(VO)_6(PO_4)_2(HPO_4)_{11} \cdot 3H_2O$

Atom	*x*	*y*	*z*	U_{eq}[a]
Ba(1)	0.19079(2)	½	0.47754(6)	0.0113
Ba(2)	0.10389(2)	0	0.21964(6)	0.0150
V(1)	0	0	½	0.0181
V(2)	0.17576(5)	½	0.9749(2)	0.0094
P(1)	0.06602(8)	½	0.4682(3)	0.0137
P(2)	0.21734(7)	1	1.1894(3)	0.0086
P(3)	0.15396(7)	0	0.7305(3)	0.0099
P(4)[b]	0.9837(5)	1	0.080(2)	0.035(3)[c]
O(1)	0.0423(2)	0.257(1)	0.4219(6)	0.0204
O(2)	0.0246(3)	0	0.724(1)	0.0363
O(3)	0.1079(2)	½	0.3757(9)	0.0170
O(4)	0.0749(3)	½	0.6717(9)	0.0305
O(5)	0.1889(1)	0.7630(9)	1.1604(5)	0.0133
O(6)	0.1263(2)	½	1.0099(8)	0.0168
O(7)	0.1779(1)	0.2402(9)	0.7869(5)	0.0137
O(8)	0.2465(2)	½	0.9437(8)	0.0183
O(9)	0.2332(2)	1	1.3734(8)	0.0135
O(10)	0.1467(2)	0	0.5395(8)	0.0151
O(11)	0.1103(2)	0	0.8298(8)	0.0180
O(20)[d]	0.4625(5)	0.254(4)	0.980(2)	0.060(4)[c]
O(21)[b]	1.033(1)	1	0.041(5)	0.036(8)[c]

[a] U_{eq} (Å^2) = $(U_1U_2U_3)^{1/3}$.
[b] Fractional site occupancy = ¼.
[c] U_{iso} (Å^2).
[d] Fractional site occupancy = ½.

TABLE 5
Selected Bond Distances (Å) for $Ba_8(VO)_6(PO_4)_2(HPO_4)_{11} \cdot 3H_2O$

Ba(1)–O(3)	2.736(7)	Ba(1)–O(5)	2.823(4) × 2
Ba(1)–O(7)	2.796(4) × 2	Ba(1)–O(9)	3.045(3) × 2
Ba(1)–O(9)	2.662(6)	Ba(1)–O(10)	2.997(4) × 2
Ba(2)–O(1)	2.853(5) × 2	Ba(2)–O(3)	2.876(3) × 2
Ba(2)–O(5)	3.004(5) × 2	Ba(2)–O(6)	3.158(4) × 2
Ba(2)–O(10)	2.823(6)	Ba(2)–O(11)	3.044(7)
Ba(2)–O(20)	2.90(2) × 2	Ba(2)–O(21)	2.63(4)
V(1)–O(1)	1.993(5) × 4	V(1)–O(2)	1.902(8) × 2
V(2)–O(5)	2.030(4) × 2	V(2)–O(6)	1.595(7)
V(2)–O(7)	1.995(4) × 2	V(2)–O(8)	2.257(7)
P(1)–O(1)	1.514(5) × 2	P(1)–O(3)	1.516(7)
P(1)–O(4)	1.606(8)		
P(2)–O(5)	1.543(5) × 2	P(2)–O(8)	1.553(7)
P(2)–O(9)	1.513(6)		
P(3)–O(7)	1.525(5) × 2	P(3)–O(10)	1.502(6)
P(3)–O(11)	1.591(7)		
P(4)–O(2)	1.56(2)	P(4)–O(20)[a]	1.64(2) × 2
P(4)–O(21)[a]	1.59(4)		

[a] Less reliable value, due to disorder.

which propagate in the **b**-direction. Ba(1) and Ba(2) polyhedra are connected via O(3) and O(10), and form their own infinite **b**-direction column.

V(1), P(1), and P(4), together with their associated oxygen atoms (Fig. 9), form the first type of polyhedral chain in $Ba_8(VO)_6(PO_4)_2(HPO_4)_{11} \cdot 3H_2O$. These chains, comprised of $V(1)O_6$ octahedra linked together by pairs of $P(1)O_4$ tetrahedra, and crosslinked by disordered $P(4)O_4$ groups, propagate in the **b**-direction. The V(1) octahedron appears to be unusual for V^{IV} in the absence of a short ($d < 1.6$ Å) V=O bond typically found for V^{IV}-containing materials (26). We believe that this central V(1) site in $Ba_8(VO)_6(PO_4)_2(HPO_4)_{11} \cdot 3H_2O$ is an average of superimposed O–V=O and O=V–O configurations: The thermal factor of the V(1) atom is highly anisotropic along the O(2)–V(1)–O(2′) axis (Fig. 9), indicating probable disorder. In the related $Ba_2VO(PO_4)_2 \cdot H_2O$ (27), which has a similar V/P/O chain configuration to the $V(1)O_6/P(1)O_4$ chain in $Ba_8(VO)_6(PO_4)_2(HPO_4)_{11} \cdot 3H_2O$, the vanadium atom is disordered over two adjacent positions (apparent V···V separation ~0.7 Å), due to superimposed H_2O–V=O and O=V–OH_2 configurations: However, the situation in $Ba_8(VO)_6(PO_4)_2(HPO_4)_{11} \cdot 3H_2O$ is further complicated by the fact that the O(2) atom represents up to *three* chemically different types of oxygen atom; a V(1)=O(2) terminal atom, a possible V(1)–O(2)H_2 water molecule oxygen atom, and a V(1)–O(2)–P(4) bridging O atom. The V(1)/P(1)/P(4) chain has $2/m$ symmetry along **b**, about the vanadium centers, at least as represented by this simplified structural model.

The other four V(1) oxygen-atom vertices link to four different phosphorus atoms, and a fairly regular octahedral geometry [d_{av}(V–O) = 1.955(3) Å] results. A BVS analysis (21) of the $V(1)O_6$ coordination sphere (Table 5) yielded a value of 3.4, apparently intermediate between (ideal) V^{III} and V^{IV} character. However, if the disorder effect described in the above paragraph is considered, by assuming bond lengths of 1.604 Å for the V=O link, and 2.200 Å for the *trans* V–O bond (split from 2 × 1.902 Å for the disordered case) and 4 × 1.993 Å for the unchanged V–O–P bonds, then a typical V^{IV} BVS of ~4.1 is obtained. This is consistent with the magnetic susceptibility data (*vide infra*) which indicate that only V^{IV} is present in $Ba_8(VO)_6(PO_4)_2(HPO_4)_{11} \cdot 3H_2O$.

The V(2)/P(2)/P(3) double chains (Fig. 10) are quite distinct from the first chain, although both are aligned in the **b**-direction. A similar double phosphate bridge, via the P(2)- and P(3)-centered groups link adjacent V(2) centers. However, V(2) does possess a short, vanadyl V=O bond [d = 1.596(7) Å] to O(6), while the long *trans* V(2)–O(8) bond [d = 2.258(7) Å] connects [via P(2)] to a similar double-bridged chain propagating one-half step out of

TABLE 6
Selected Bond Angles (°) for $Ba_8(VO)_6(PO_4)_2(HPO_4)_{11} \cdot 3H_2O$

O(1)–V(1)–O(1)	180[a]	O(1)–V(1)–O(1)	95.7(3)
O(1)–V(1)–O(1)	84.3(3)	O(1)–V(1)–O(2)	90.5(3)
O(1)–V(1)–O(2)	89.5(3)	O(2)–V(1)–O(2)	180[a]
O(5)–V(2)–O(5)	84.9(3)	O(5)–V(2)–O(6)	94.2(2)
O(5)–V(2)–O(7)	166.2(2)	O(5)–V(2)–O(7)	93.2(2)
O(6)–V(2)–O(7)	99.6(2)	O(7)–V(2)–O(7)	85.4(3)
O(5)–V(2)–O(8)	83.1(2)	O(6)–V(2)–O(8)	176.4(3)
O(7)–V(2)–O(8)	83.1(2)		
O(1)–P(1)–O(1)	113.5(4)	O(1)–P(1)–O(3)	108.8(2)
O(1)–P(1)–O(4)	108.4(3)	O(3)–P(1)–O(4)	108.9(5)
O(5)–P(2)–O(5)	106.3(4)	O(5)–P(2)–O(8)	109.6(2)
O(5)–P(2)–O(9)	109.0(2)	O(8)–P(2)–O(9)	113.0(4)
O(7)–P(3)–O(7)	110.2(4)	O(7)–P(3)–O(10)	110.9(2)
O(7)–P(3)–O(11)	107.0(2)	O(10)–P(3)–O(11)	110.8(4)
O(2)–P(4)–O(20)	113.0(9)	O(2)–P(4)–O(20)	110.5(8)
O(20)–P(4)–O(20)	102.9(14)	O(2)–P(4)–O(21)	111.4(17)
O(20)–P(4)–O(21)	108.0(11)	O(20)–P(4)–O(21)	101.1(19)
V(1)–O(1)–P(1)	145.3(3)	V(1)–O(2)–P(4)	146.0(8)
V(2)–O(5)–P(2)	139.4(3)	V(2)–O(7)–P(3)	138.4(3)
V(2)–O(8)–P(2)	144.4(4)		

[a] By symmetry.

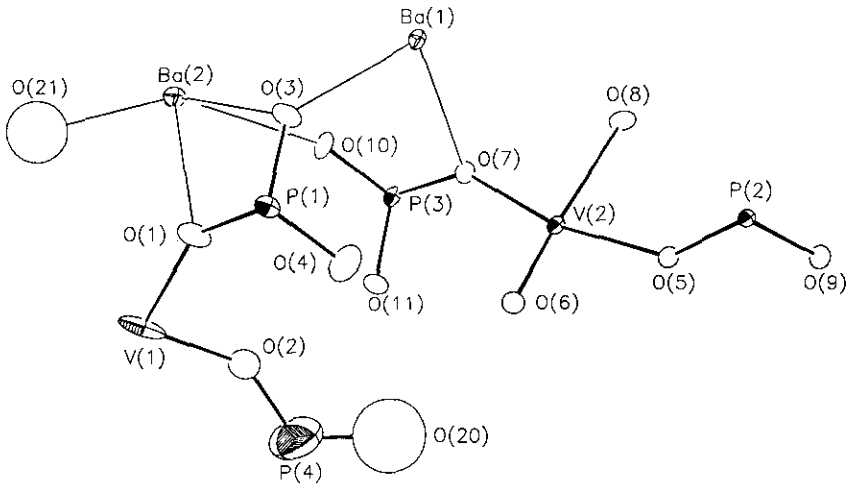

FIG. 5. ORTEP view of the V/P/O asymmetric unit of $Ba_8(VO)_6(PO_4)_2(HPO_4)_{11} \cdot 3H_2O$, showing the atom-labeling scheme (50% thermal ellipses).

phase with the first chain. Terminal P–O links to O(9), O(10), and O(11) bond to no other V/P species, but do form part of the Ba^{2+} coordination polyhedron (Table 5). O(11) is probably protonated, as indicated by the lengthened P(3)–O(11) bond distance (Table 5). A BVS calculation for V(2) gave a satisfactory value of 4.1 (expected 4.0), assuming that the site has V^{IV} character. Overall, this second chain has $2_1/m$ symmetry along **b**, and is completely isolated from the first chain, except for nonbonding links via barium cations.

INFRARED SPECTROSCOPY

The IR spectrum of $Ba(VO)_2(SeO_3)_2(HSeO_3)_2$ is shown in Fig. 11. The band at 950 cm^{-1} is due to V=O, while bands at 825, 781, and 700 cm^{-1} arise from selenite-group vibrations (28). The sharp resonance at 1217 cm^{-1} probably arises from an Se–O–H vibration. The IR spectrum of $Ba_8(VO)_6(PO_4)_2(HPO_4)_{11} \cdot 3H_2O$ is shown in Fig. 12. As well as characteristic PO_4 and V=O bands (1106 cm^{-1}, 967 cm^{-1}, and 590 cm^{-1}) the data show a band arising from the presence of a coordinated water molecule (ν = 1636 cm^{-1}), which may be bonded to either Ba or V.

MAGNETIC MEASUREMENTS

Susceptibility data for $Ba(VO)_2(SeO_3)_2(HSeO_3)_2$ (Fig. 13) showed perfect Curie behavior over the complete 4–300 K range, with no evidence for any cooperative magnetic phenomena. The data were modeled by using a Curie–Weiss type law; $\chi = \chi_0 + C/(T - \theta)$, where χ is the measured magnetic susceptibility, C is the Curie constant, T the temperature (K), and θ the Weiss constant. The model yield values of $\chi_0 = -5.685 \times 10^{-8}$ emu/g, $C = 1.115 \times 10^{-3}$ emu-K/g, and $\theta = 0$ K, corresponding

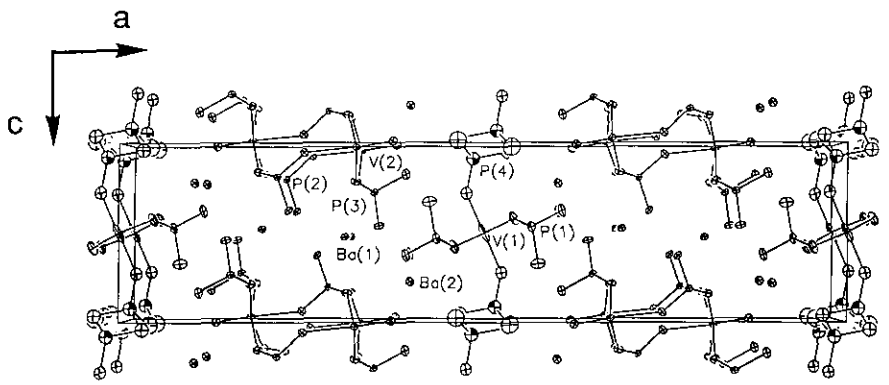

FIG. 6. Unit-cell packing of $Ba_8(VO)_6(PO_4)_2(HPO_4)_{11} \cdot 3H_2O$, viewed down the **b**-direction. The $P(4)O_4$ phosphate groups are disordered (see text).

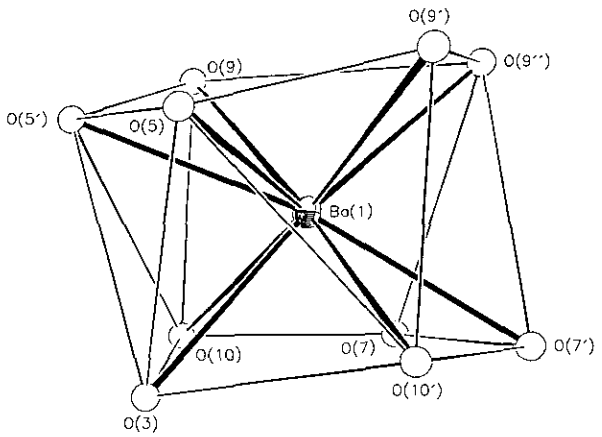

FIG. 7. Tenfold Ba(1) coordination polyhedron in $Ba_8(VO)_6(PO_4)_2(HPO_4)_{11} \cdot 3H_2O$, with non-bonding O· · ·O contacts <3.6 Å indicated by thin lines (see text).

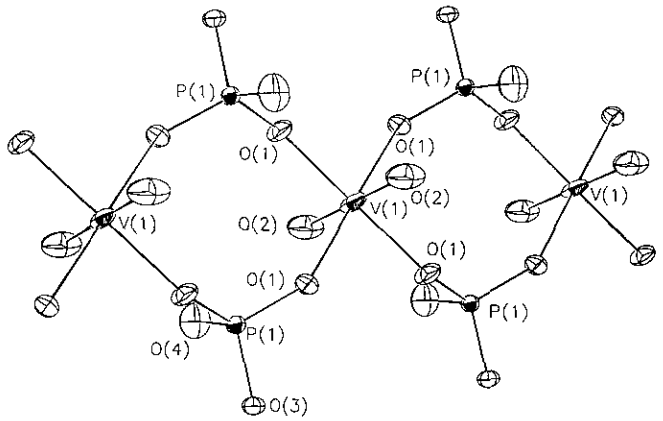

FIG. 9. View of the vanadium(IV)-containing V(1)/P(1) chain in $Ba_8(VO)_6(PO_4)_2(HPO_4)_{11} \cdot 3H_2O$; the chain axis points in the **b**-direction. Disordered $P(4)O_4$ groups are attached to oxygen atom O(2).

to a μ_{eff} of 1.86 BM (spin-only value for vanadium(IV) = 1.73 BM).

$Ba_8(VO)_6(PO_4)_2(HPO_4)_{11} \cdot 3H_2O$ shows a maximum in its inverse susceptibility at ~20 K (Fig. 14), presumably corresponding to antiferromagnetic ordering, along either the $V(1)^{IV}$ chain or the double chain of $V(2)^{IV}$ centers. In the range 100–300 K, the data were modeled by a Curie–Weiss law, resulting in parameters of $\chi_0 = 4.729 \times 10^{-7}$ emu/g, $C = 7.578 \times 10^{-4}$ emu-K/g, and $\theta = -30.4$ K. The higher temperature data yielded a $\mu_{eff} = 2.92$ BM in good agreement with the predicted value of 3.00 BM, for three noninteracting spin-only V^{IV} sites.

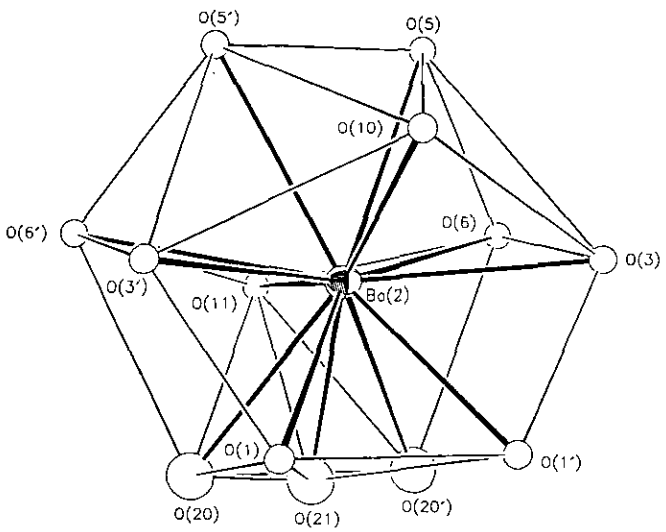

FIG. 8. Thirteenfold Ba(2) coordination polyhedron in $Ba_8(VO)_6(PO_4)_2(HPO_4)_{11} \cdot 3H_2O$, with non-bonding O· · ·O contacts <4.0 Å indicated by thin lines. Disordered oxygen atoms (Table 4) are represented by larger spheres.

The closest vanadium–vanadium distances in the two V/P/O chains are identical: 5.208 Å for both the V(1) chain and the V(2) double chain. A second V(2)–V(2) contact at 5.39 Å is present in the V(2) double chain. These contacts are far too large to allow for direct, through-space magnetic coupling between adjacent V atoms, thus the superexchange pathway must be via V–O–P–O'–V' links. Antiferromagnetic ordering at low temperature (~10 K) is also observed in $Ba_2VO(PO_4)_2 \cdot H_2O$ (27), which has a similar one-dimensional V/P/O configuration to the V(1) chain in $Ba_8(VO)_6(PO_4)_2(HPO_4)_{11} \cdot 3H_2O$.

CONCLUSION

$Ba(VO)_2(SeO_3)_2(HSeO_3)_2$ and $Ba_8(VO)_6(PO_4)_2(HPO_4)_{11} \cdot 3H_2O$ further expand the wide variety of known framework phases containing octahedral vanadium cen-

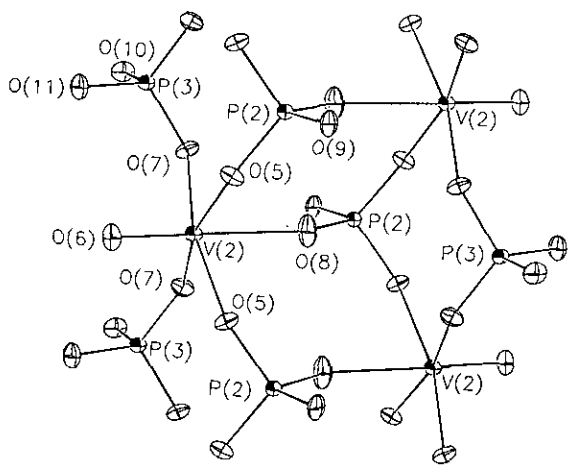

FIG. 10. View of the vanadium(IV)-containing V(2)/P(2)/P(3) chain in $Ba_8(VO)_6(PO_4)_2(HPO_4)_{11} \cdot 3H_2O$.

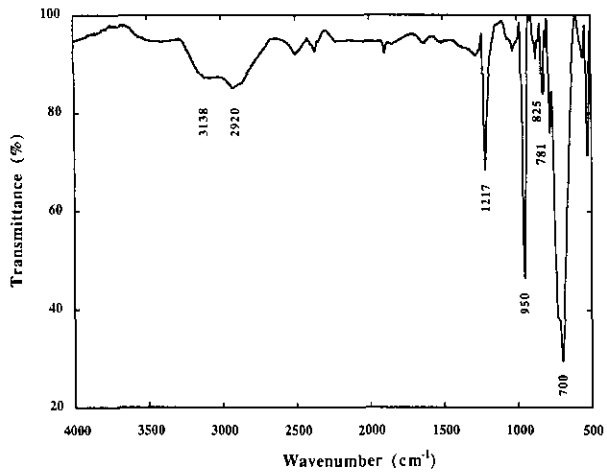

FIG. 11. Infrared spectrum of $Ba(VO)_2(SeO_3)_2(HSeO_3)_2$, with major bands labeled.

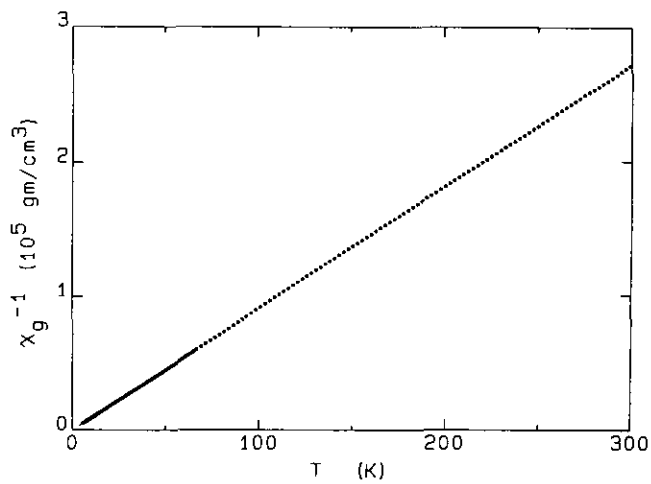

FIG. 13. Magnetic susceptibility data for $Ba(VO)_2(SeO_3)_2(HSeO_3)_2$, plotted as $1/\chi$ versus temperature.

ters and other linking polyhedra. As expected, in $Ba(VO)_2(SeO_3)_2(HSeO_3)_2$, SeO_3 ions form triangular bridges between vanadium centers, although protonated Se–OH terminal bonds may also occur. A three-dimensional structure results, and a pure V^{IV} character is well defined for the vanadium centers in this phase. No cooperative magnetic ordering occurs above 4 K.

In $Ba_8(VO)_6(PO_4)_2(HPO_4)_{11} \cdot 3H_2O$, the combination of $V^{IV}O_6$ centers with $(H)PO_4$ tetrahedra leads to a structure with a strong one-dimensional character, with two completely separate types of V/P/O chains formed. One of the V sites is disordered between O=V–O and O–V=O configurations, which wrongly suggests a partial V^{III} character: Magnetic susceptibility data indicate only V^{IV} is present in this material, and antiferromagnetic ordering occurs below ~20 K.

Interesting related structures include the novel V^{III}/V^{IV} phases $K(VO)V(HPO_4)_3(H_2O)_2$ (11) and $K_2(VO)_2V(PO_4)_2(HPO_4)(H_2PO_4)(H_2O)_2$ (29). Both of these materials contain structurally distinct V^{III} and V^{IV} octahedral centers; the latter phase forms a "staircase" layered structure. Our own synthetic and structural studies of complex vanadium selenities and phosphates are continuing and will be reported later.

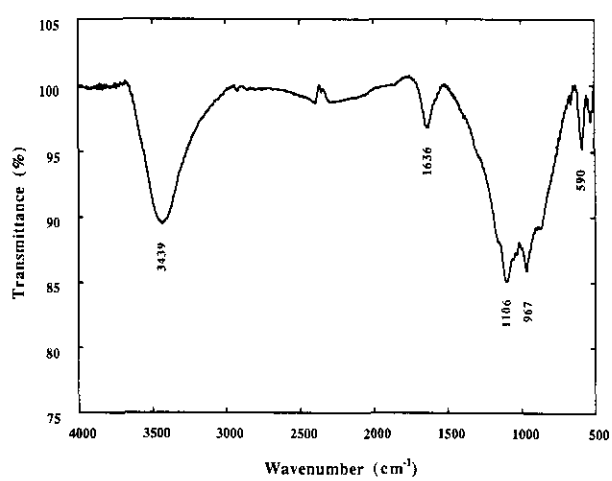

FIG. 12. Infrared spectrum of $Ba_8(VO)_6(PO_4)_2(HPO_4)_{11} \cdot 3H_2O$, with major bands labeled, including the bound-water resonance at 1636 cm^{-1} (see text).

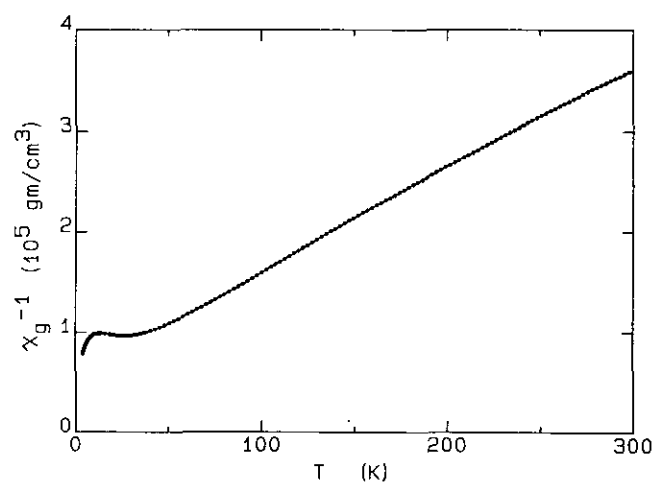

FIG. 14. Plot of $1/\chi$ versus temperature for $Ba_8(VO)_6(PO_4)_2(HPO_4)_{11} \cdot 3H_2O$.

ACKNOWLEDGMENTS

We thank Jim Korp and Ivan Bernal (University of Houston) for assistance with the X-ray data collections. This work is funded by the National Science Foundation (DMR 9214804) and the R. A. Welch Foundation.

REFERENCES

1. P. B. Moore and J. Shen, *Nature (London)* **306,** 356 (1983).
2. T. Loiseau and G. Férey, *Chem. Commun.* 1197 (1992).
3. W. T. A. Harrison, T. E. Gier, and G. D. Stucky, *Angew. Chem. Int. Ed. Engl.* **32,** 724 (1993).
4. L. A. Mundi, K. G. Strohmaier, and R. C. Haushalter, *Inorg. Chem.* **30,** 154 (1991).
5. R. C. Haushalter and L. A. Mundi, *Chem. Mater.* **4,** 31 (1992), and included references.
6. H. R. Tietze, *Aust. J. Chem.* **34,** 2035 (1981).
7. J. W. Johnson and A. J. Jacobson, *Angew. Chem. Int. Ed. Engl.* **22,** 412 (1983).
8. S. L. Wang, H. Y. Kang, C. Y. Cheng, and K. H. Lii, *Inorg. Chem.* **30,** 3496 (1991).
9. K. H. Lii, N. S. Wen, C. C. Su, and B. R. Chen, *Inorg. Chem.* **31,** 439 (1992).
10. V. Soghomonian, Q. Chen, R. C. Haushalter, J. Zubieta, and C. J. O'Connor, *Science (Washington, D.C.)* **259,** 1596 (1993).
11. R. C. Haushalter, Z. Wang, M. E. Thompson, and J. Zubieta, *Inorg. Chem.* **32,** 3700 (1993), and included references.
12. G. Huan, J. W. Johnson, A. J. Jacobson, E. W. Corcoran, Jr., and D. P. Goshorn, *J. Solid State Chem.* **93,** 514 (1991).
13. J. T. Vaughey, W. T. A. Harrison, A. J. Jacobson, D. P. Goshorn, and J. W. Johnson, *J. Solid State Chem.* **110,** 305 (1994).
14. G. Huan, J. W. Johnson, A. J. Jacobson, D. P. Goshorn, and J. S. Merola, *Chem. Mater.* **3,** 539 (1991).
15. M. E. Leonowicz, J. W. Johnson, J. F. Brody, H. F. Shannon, Jr., and J. M. Newsam, *J. Solid State Chem.* **56,** 370 (1985).
16. G. M. Sheldrick, "SHELXS-86 User Guide." Crystallography Department, University of Göttingen, Germany, 1986.
17. N. Walker and D. Stuart. *Acta Crystallogr. Sect. A* **39,** 158 (1983).
18. A. C. Larson, *Acta Crystallogr.* **23,** 664 (1967).
19. "International Tables for X-Ray Crystallography," Vol. IV. Kynoch Press, Birmingham, 1974.
20. D. J. Watkin, J. R. Carruthers, and P. W. Betteridge, "CRYSTALS User Guide." Chemical Crystallography Laboratory, Oxford University, United Kingdom, 1985.
21. A. J. Jacobson, J. W. Johnson, J. F. Brody, J. C. Scanlon, and J. T. Lewandowski, *Inorg. Chem.* **24,** 1782 (1985).
22. N. E. Brese and M. O'Keefe, *Acta Crystallogr. Sect. B* **47,** 192 (1991).
23. W. T. A. Harrison, G. D. Stucky, and A. K. Cheetham, *Eur. J. Solid State Inorg. Chem.* **30,** 347 (1993).
24. R. E. Morris, A. P. Wilkinson, and A. K. Cheetham, *Inorg. Chem.* **31,** 4775 (1992).
25. R. E. Morris and A. K. Cheetham, *Chem. Mater.* **6,** 67 (1994).
26. R. Gopal and C. Calvo, *J. Solid State Chem.* **5,** 432 (1972).
27. W. T. A. Harrison, S. C. Lim, J. T. Vaughey, A. J. Jacobson, D. P. Goshorn, and J. W. Johnson, *J. Solid State Chem.* **113,** 444 (1994).
28. R. E. Morris, W. T. A. Harrison, G. D. Stucky, and A. K. Cheetham, *J. Solid State Chem.* **94,** 227 (1991).
29. R. C. Haushalter, Z. Wang, M. E. Thompson, J. Zubieta, and C. J. O'Connor, *Inorg. Chem.* **32,** 3966 (1993).